Materials and Design 163 (2019) 107544

Contents lists available at ScienceDirect

Materials and Design

journal homepage: www.elsevier.com/locate/matdes

4D printing with robust thermoplastic polyurethane hydrogel-elastomer trilayers

Anna B. Baker[a,b], Simon R.G. Bates[a,b,*], Thomas M. Llewellyn-Jones[a,b], Laurie P.B. Valori[b], Michael P.M. Dicker[a], Richard S. Trask[a,b]

[a] Bristol Composites Institute (ACCIS), School of Civil, Aerospace and Mechanical Engineering (CAME), University of Bristol, Bristol BS8 1TR, UK
[b] Mechanical Engineering, University of Bath, Claverton Down, Bath BA2 7AY, UK

HIGHLIGHTS

- Thermoplastic polyurethane hydrogel filament was manufactured and 3D-printed into multi-material structures.
- A range of trilayer constructs with hydration-triggered hydrogel hinges were produced using low-cost desktop 3D printers.
- The effect of varying hinge geometry on the final actuation angle and the transient actuation progression was investigated.
- Complex tessellated origami structures were produced which had not been previously realised by 4D-printing.

GRAPHICAL ABSTRACT

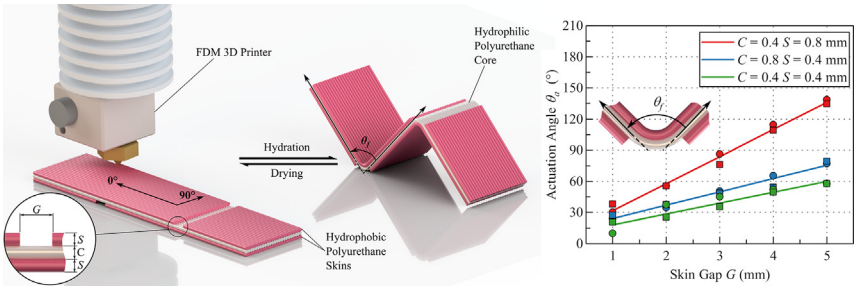

ARTICLE INFO

Article history:
Received 29 October 2018
Received in revised form 7 December 2018
Accepted 8 December 2018
Available online 13 December 2018

Keywords:
4D printing
Hydrogels
Thermoplastic polyurethane
Trilayers
Origami
Active structures

ABSTRACT

Here we present a new 4D printing technique capable of producing a diverse range of trilayer constructs using commercial low-cost desktop 3D printers. This unique methodology permits the viable construction of dynamically robust and complex origami architectures for a new generation of active structures. The resulting creations transform from flat 2D parts to 3D structures through submersion in water and return to their original configuration through dehydration. This technique uses commercially available materials and printers to enable a 4D printing method that is more accessible and affordable than previous examples of hydration triggered 4D printing. This method yields a controlled and predictable actuation route and final shape, enabling it to be used for both simple and complex origami inspired designs, such as the tessellated waterbomb origami pattern, a design that has not previously been realised with 4D printing. These new designs demonstrate how the integration of multiple trilayers into a single 3D print enables through-thickness control of actuation and resulting formation of active structures with complexity beyond what has previously been achieved with 4D printing.

1. Introduction

The emerging field of 4D printing has rapidly developed over the last decade and combines the areas of 3D printing with smart materials and design to enable the creation of 3D printed objects that evolve over time in response to their environment [1]. Through the use of 4D printing, the manufactured and final form of a part are different,

* Corresponding author.
E-mail addresses: a.b.baker@bristol.ac.uk (A.B. Baker), s.r.g.bates@bristol.ac.uk (S.R. Bates), r.s.trask@bristol.ac.uk (R.S. Trask).

https://doi.org/10.1016/j.matdes.2018.107544

enabling each to be optimised for a different purpose. For example, the initial shape may be tailored for manufacturing and transportation, while the final 3D shape may be designed for its ultimate function. 4D printing has the potential to be used for stimuli-responsive devices (valves and grabbers), smart origami (stents and 3D polygons) and in-situ assembly (packing and encapsulation) applications in the fields of robotics, biomedical science and architecture [2-6]. 4D printing has been demonstrated through the use of a variety of smart materials, including shape memory polymers (SMP), liquid crystal elastomers (LCE) and hydrogels [1,2,4,5, 7-11]; with these materials fabricated through a range of 3D printing techniques, such as stereolithography, fused filament fabrication (FFF) and PolyJet printing [12].

FFF 3D printing is the most affordable, accessible and versatile of all the 4D printing techniques, forming printed structures via layer wise deposition of melted and subsequently cooled thermoplastic polymers [13]. 3D printing enables automated, high-resolution spatial control over the location of multiple materials within a single construct. FFF 3D printers are the most commonly used by hobbyists, being a low-cost machine that is compatible with a wide range of low-cost materials. FFF enables the printing of a range of materials with diverse physical and mechanical properties. Thermoplastic polyurethane (TPU) materials have been used within FFF printing to create flexible and robust 3D printed parts, with Ninjaflex®, a TPU filament manufactured by Fenner Drives®, being used previously in energy absorption, soft-robotics and prosthetics applications [14-17]. While Ninjaflex is a hydrophobic TPU, various hydrophilic TPU materials are also available. While these hydrogels have not generally been applied to FFF printing, they have found use in active materials research [18-20]. One such commercially available hydrogel is Tecophilic™, a hydrophilic Lubrizol manufactured pellet, used previously in drug delivering devices, antimicrobial wound dressing and tissue engineering [21-23].

Both solution based and photo-polymerised 3D printing of hydrogel materials have been demonstrated, with combinations of both passive and stimuli-responsive materials, through fibre reinforcements, discrete material deposition and photoinduced differential in crosslinking density being used to realise the final 4D printed functionality [9-11]. While these techniques have resulted in impressive demonstrations, they have all involved custom or specialised 3D printers and materials.

Bilayer hydrogel based materials have been widely studied in 4D printing [6,11,24,25]. Bilayers have been constructed by combining layers of active hydrogel material and passive polymeric materials. Shape change of the bilayer is achieved by the relative change in volume of the two layers through water absorption in the active material. These changes in hydration can be triggered by environmental stimuli such as temperature, pH, light or humidity [26-31]. Bilayers usually shape change from their flat configuration to curved arcs, with radius of curvature determined by the relative stiffness, expansion and thicknesses of the two adjoined materials. The relationship of these variables was described by Timoshenko and has been shown to accurately predict the behaviour of hydrogel based bilayers [9,32-36]. Though trilayer constructions (passive skins and an active hydrogel core) have been shown to remain flat upon hydration of the hydrogel layer (due to the symmetry of the trilayer construction), the combination of a global trilayer with localised bilayer hinges has been shown on a microscale using complex and labor intensive processes to be an effective method of creating hydrogel based origami structures [37,38].

2. Experimental methods and results

Here, we demonstrate 4D printed origami-inspired structures formed from a global trilayer composition (passive) with localised bilayer regions (active hinges). Through combining bilayers and trilayers (polyurethane hydrogel cores with polyurethane elastomer skins) within a single print, shape-change upon hydration of the hydrogel is observed, with the change in shape determined by the spatial location of the bilayers within the structure. FFF 3D printing of these sandwich structures enables this spatial control within a simple and rapid manufacturing technique (Fig. 1).

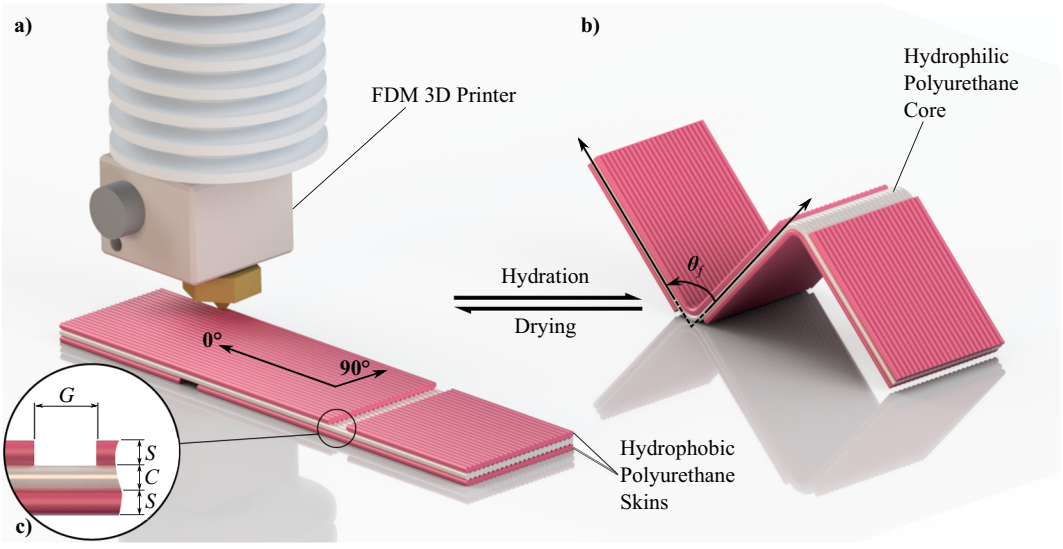

Fig. 1. The multi-material trilayers consist of hydrophobic polyurethane top and bottom skins (pink), with a hydrophilic polyurethane core (white). a) All materials are 3D printed with a low-cost desktop Fused Filament Fabrication (FFF) machine. The skin print paths at either 0° or 90° in this study (here shown at 0°) are defined with respect to the core print path direction, which always takes the shortest route over the skin gaps. b) Following printing and upon hydration the trilayer bends out-of-plane at the location of the skin gaps. The angle of the fold created is defined as θ_f, a value that will return to 180° (flat) upon drying. c) The amount of bending can be controlled by changing the gap width *G* and the skin and core thickness *S* and *C*.

The bilayer construction forms the active component of the 3D printed part and its dimensions and composition will determine the hydrated shape it forms. This study utilised a single active hydrogel (Tecophilic™ TPU (HP-93A-100)), and a single passive elastomer (NinjaFlex 85A). The properties of these two materials are shown in Table 2. Custom hydrogel filament was manufactured from dried Tecophilic TPU pellets (80°C, 5 h at 60 mbar) with a filament extruder (FilaFab Pro Ex Extruder, 2.5 mm nozzle) with a diameter of 2.85 mm (±0.05 mm) at 190°C and wound on a custom built filament winder. In this study the only variable affecting the radius of curvature during actuation is the thickness of each layer. However, the length of the arc can also be controlled by varying the length of the bilayer. A combination of these variables was investigated to determine the ability of the bilayer to form a hinge with a predictable actuation angle. The bilayer dimensions investigated consist of individual layer thicknesses of 0.4 or 0.8 mm, bilayer lengths of 1, 2, 3, 4 and 5 mm, and bilayers printed forming valley or mountain folds, through missing a material channel in either bottom or top elastomer layers, respectively (Fig. 2a and b) in the printing process. Sample sets were printed using an Ultimaker Original+ 3D printer with a Flex3Drive direct-drive extruder, using a single E3D print nozzle. Print settings for both materials are shown in Table 1. Prints were performed with the skin toolpath either along the sample length (0°) or transverse to the sample length (90°), to determine whether anisotropy in the skins would affect the actuation of each hinge. As seen in Fig. 2, there is a negligible difference in the actuation angle between the (0°) and (90°) samples, showing that skin print orientation does not affect actuation performance. Valley folds are forming by printing an open channel in the first layer (or first and second for 0.8 mm elastomer/skin thickness) at the required hinge location, while mountains folds are formed by printing an open channel in the final layer (or final two layers for 0.8 mm elastomer/skin thickness) as shown in Fig. 1c, here after referred to as skin gaps with a width, G (mm).

Through increasing bilayer length *i.e.* gap length, the actuation angle formed increased in a linear fashion due to increasing arc length. This trend can be seen across the various thickness and fold directions, (Fig. 2a and b). The thickness of each layer affected the radius of curvature, with samples with layers of the same thickness (0.4 mm hydrogel and 0.4 mm elastomer) showing the smallest radius of curvature *i.e.* producing the greatest actuation angles, both for top and bottom skin gaps. The location of the skin gap also affected the actuation angle formed, with skin gaps located on the top surface (mountain folds) forming larger angles than gaps located on the bottom surface (valley folds). The origin of this difference arises from the way in which the valley fold is printed; the layer of hydrogel is printed across the gap, as opposed to over a layer of elastomer as with the rest of the print, which results in sagging of the hydrogel into the gap and therefore increased deposition of the hydrogel, due to a reduction in back-pressure at the print nozzle. Both of these differences are likely to affect the hydrated shape of the bilayer. However, the resulting actuation angle of valley fold, like a mountain fold, is both repeatable and predictable. As a result, the data gathered here can be used as a design tool for creating predictable shape change. Through using hydrogel and elastomer layer thicknesses of 0.4 mm and skin gap sizes between 1 and 5 mm, mountain and valley folds with actuation angles of between 43–191° and 32–136° can be achieved, respectively.

The rate at which the curvature is formed was investigated (Fig. 3) using a mountain fold with C and S values of 0.4 mm and 0.4 mm for all samples. The hinge is formed via hydration of the hydrogel layer, with the rate of hydration determined by the diffusion of the water through the hydrogel. Initially the hinges fold relatively quickly, achieving 25% of the final angle within 3 min, while taking 13, 32 and 360 min(6 h) to reach a fold with 50, 75 and 100% of

Table 1
Print settings used to manufacture all samples within this study.

Print setting	Value	Unit
Nozzle diameter	0.8	mm
Layer thickness	0.4	mm
Nozzle temperature	230	°C
Bed temperature	70	°C
Print speed	20	mm s^{-1}
Ninjaflex flow	80	%
Tecophillic TPU	90	%

Table 2
Material properties of polyurethanes used for 3D printing.

	Elastomer	Hydrogel
Manufacturer	Fenner drives	Lubrizol
Product name	NinjaFlex 3D Printing filament	Tecophilic extrusion HP-93A-100
T_g(°C)	−35[1]	−47[2]
T_m(°C)	216[1]	44.4, 129.2[2]
Water absorption (%)	0.22[1]	100[3]
Modulus (MPa)	12(Tensile)[1]	20(Flexural)[3]
Elongation at break (%)	660	1040 (dry)/620 (wet) [3]

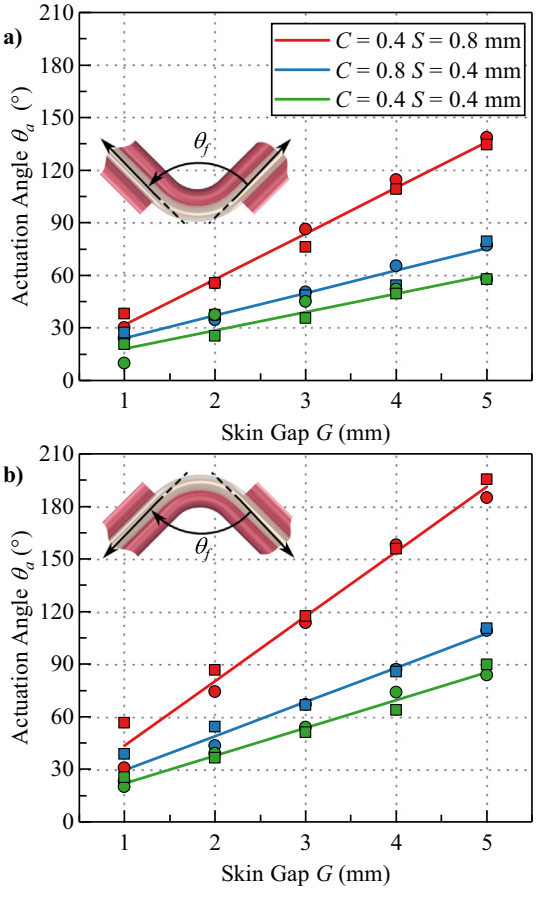

Fig. 2. Hydrated out-of-plane actuation angle ($\theta_a = 180 - \theta_f$) formed with variable gap size (G = 1–5 mm), hydrogel core (C, white) and elastomer skin (S, pink) dimensions (mm). a) Gap on bottom surface & b) gap on top surface. Key: circle=0° & square=90° skin print paths.

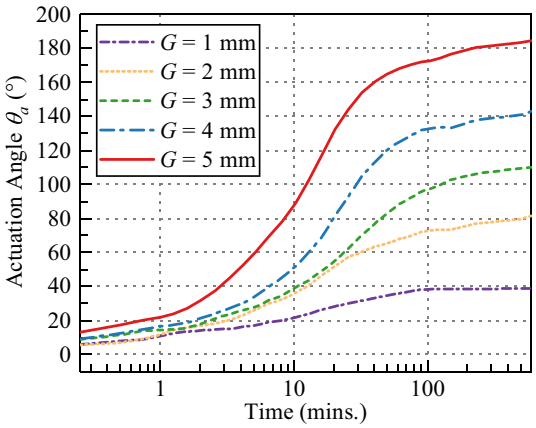

Fig. 3. Change in actuation angle ($\theta_a = 180 - \theta_f$) over time (11 h), for variable top skin gap size (G = 1–5 mm).

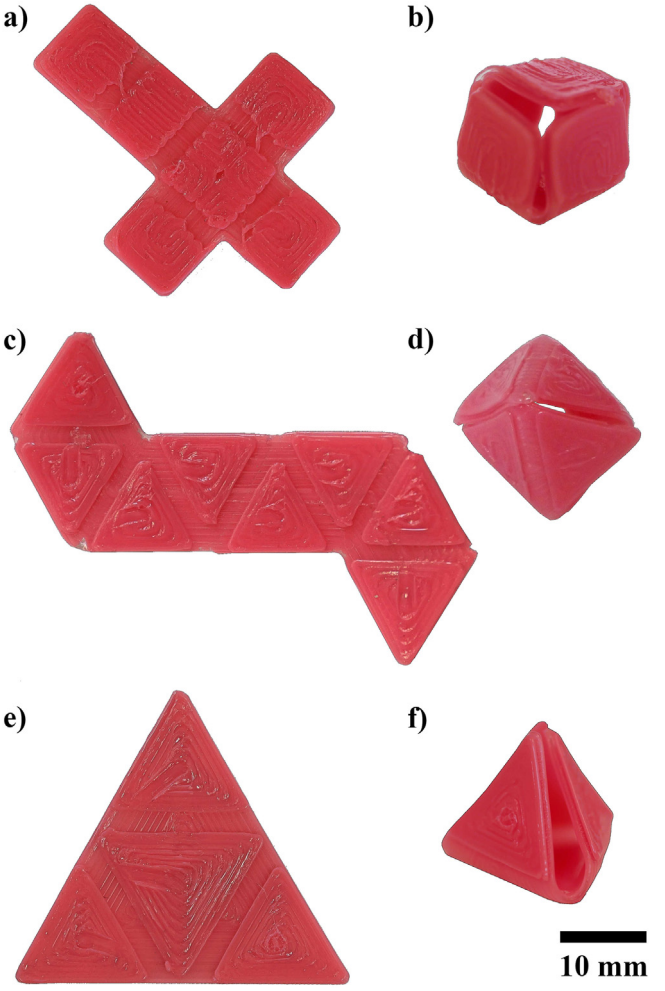

Fig. 4. Actuation of polygons from dehydrated (left) to hydrated (right); a) cruciform to d) cube; b) octagon to e) octahedron and c) triangle to f) tetrahedron. All images taken of samples in air.

the actuation angle, respectively. This trend was observed across all gap sizes. This correlates with the water absorption properties of the hydrogel, with volume change following a logarithmic trend due to diffusion obeying Fick's law [39].

Initially, designs containing hinges of all the same direction were manufactured *i.e.* either all mountain or all valley folds; these designs formed either 3D polygons or spirals architectures (Figs. 4 and 5). The 3D polygons printed and actuated were a cube, an octahedron and a tetrahedron formed from their net shapes and requiring actuation angles of 90, 90/109 and 109°, respectively. The 3D polygons were all formed using mountain folds (top skin gaps) which allowed smaller skin gap sizes to be used to achieve the required folding (see ESI (Fig. S1, S2 and S3) for print paths). These 3D polygons demonstrate the ability to print flat composite constructions, which predictably actuate to a 3D shape. The shapes demonstrated involve a range of angles and multiple folds within a single printed construct.

Spirals, both in-plane and out-of-plane, were demonstrated using the 4D printing technique (Fig. 5); again all hinges were printed with skin gaps in the top surface, resulting in all mountain folds (see ESI (Fig. S4 and S5) for print paths). The spirals demonstrated the ability to control both the radius and pitch of spiral via skin gap size and spacing, and skin gap angle relative to length of strip (dry), respectively. All the samples shown in Figs. 4 and 5 had been through multiple hydration-dehydration cycles and showed consistent actuation behaviour with each subsequent cycle. The examples demonstrated here are two possible spiral designs, however the use of 3D printing enables an endless combination of variable pitch and radius along with continually changing pitch and radius all within a single print (Fig. 5d), with designs constrained by printable parameters. While thicker structures may be manufactured using this process, the issue of printing the active layer over gaps in the inactive layer would be exacerbated, as the material would sag further. This in turn would reduce the inter-layer adhesion between the material in subsequent layers. While the spatial resolution of the print head is 12 μm, the resolution of printed parts is limited by the use of a 0.8 mm diameter nozzle.

Origami often uses intersecting folds (vertex) to form active hinges, with the actuation angle of each hinge relating to its adjoining hinges. The rules of origami state that the sum of all the angles between folds is 360° (2π) (Kawasaki-Justin theorem) [40] and that the difference between the number of mountain and the number of valley hinges at a vertex must be 2 (Maekawa's theorem), *i.e.* M-V=±2 [41] . Examples of tessellating origami structures (nature of vertex *i.e.* mountain + valley or valley + mountain) include the square-twist (3+1), Miura-ori (3+1), waterbomb (4+2) and Kresling (4+2) with many of these designs being incorporated into smart structures through the integration of smart materials such as shape memory polymers, hydrogels and shape memory alloys [42-47]. Here we demonstrate both the Miura-ori and waterbomb designs containing 3+1 vertices for Miura-ori and 4+2 and 2+4 vertices for the waterbomb (Fig. 6) with different skin gap widths/actuation angles used to fold the origami designs to various extents (Fig. 7).

The Miura-ori origami design has been extensively studied, with the mathematics of its folding being well understood. The pattern allows significant space saving if stowing a flat construct and as a result has been incorporated into a number of smart materials to create deployable structures [5,37,48-51]. The Miura-ori design is formed with a 4 hinge intersecting vertex, with 3 hinges of mountain nature and 1 hinge of valley nature (or *vice versa*). The design used here has a high level of symmetry, with intersection vertices containing 1 mountain (θ_1) and 1 valley (θ_3) fold along the vertical, forming a line of symmetry, and 2 mountain folds (θ_4 and θ_2) at an angle of 45° (A) from the valley fold, see Fig. 6a. The actuation angle each hinge forms are dependent on each other and for the Miura-ori, which has

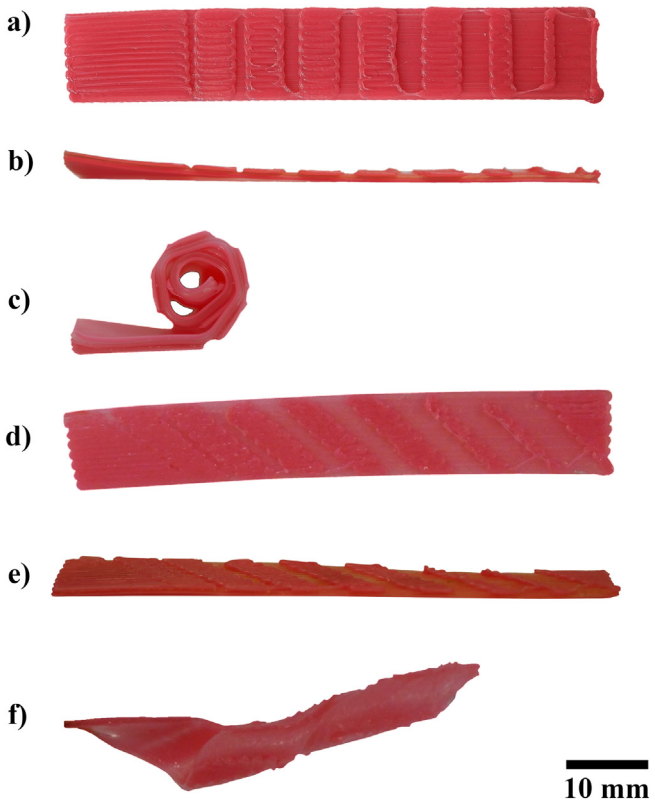

Fig. 5. Actuation of spiral strips from dehydrated to hydrated; in-plane spiral with increasing actuation angle (left to right) a) & b) dehydrated (side & top view) and c) hydrated (side view) and out-of-plane spiral with increasing actuation angle (left to right) d) & e) dehydrated (side & top view) and f) hydrated (side view). All images taken of samples in air.

a line of symmetry, is determined by Eq. (1) [52].

$$\frac{\tan(\theta_1/2)}{\tan(\theta_2/2)} = \cos(A) \tag{1}$$

Where θ_1=-θ_3 and θ_2=θ_4. By defining S and θ_1 the remaining angles and the required gap sizes were determined using the lines of best fit (Fig. 2a and b) for top and bottom gaps for constructs with 0.4 mm layers, see Table 3 (see ESI (Fig. S6 and S7) for print paths).

The waterbomb origami design has found a number of practical applications including medical stents, robotic animals (*e.g.* worm) and deployable wheels [46,53,54]. The origami waterbomb design has two different types of interconnecting hinges; firstly, an intersect formed of 2 mountain and 4 valley folds (Fig. 6b) and secondly, an intersection formed of 4 mountains and 2 valley folds (Fig. 6c). Two different waterbomb designs were 3D printed with different dimensions and intersection design (Table 4). The actuation angles are all interlinked, with these relationships determined by Eqs. (2),(3),(4),(5).

$$\tan(\phi_{f1}/2) = \sqrt{2}\tan(\phi_{f3}/2) \tag{2}$$

$$\tan(\phi_{f2}/2) = \frac{\tan(\phi_{f3}/2)}{\sqrt{2}} \tag{3}$$

$$\tan(\phi_{f4}/2) = \frac{2\tan^5(\phi_{f3}/2)}{3\sqrt{2}\tan^4(\phi_{f3}/2) + 2\sqrt{2}\tan^2(\phi_{f3}/2)} \tag{4}$$

$$\tan(\varphi_{f1}/2) = \sqrt{2}\tan(\varphi_{f2}/2) \tag{5}$$

Where A, B and C all are 45°, for full general equations see supplementary information or Chen et al. [55]. The high level of symmetry of the waterbomb designs results in a number of actuation angles being the same. The folds with the same actuation angles are shown in Table 4.

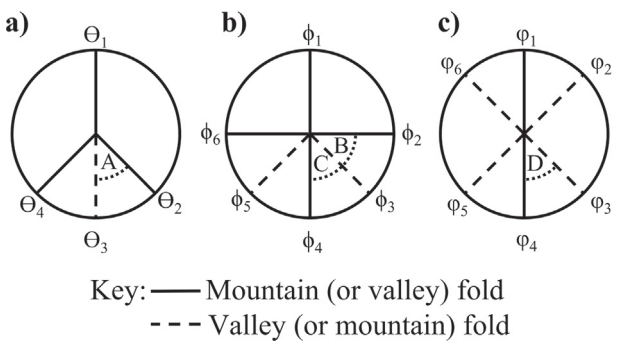

Fig. 6. Diagram of intersecting vertex for Miura-ori and waterbomb origami patterns with out-of-plane actuation angles, *i.e.* 0° = flat. a) Miura-ori intersection (3+1). b) Waterbomb 1 intersection (4+2). c) Waterbomb 2 (2+4).

3. Discussion

The two waterbomb designs successfully demonstrated the ability of this 4D printing technique to be applied to origami designs with a range of interesting and highly complex hinge arrangements (see ESI (Fig. S8 and S9) for print paths). This demonstrated that while the concept is low-cost and accessible, this does not result in a compromise of the quality or complexity of the structures that can be produced. The actuation of the hinges occurs due to local bilayers within the global trilayer construct, which forms an asymmetric cross section which bends due to the differential swelling of the two layers.

All examples demonstrated previously have controlled the location and direction of hinges using a single bilayer/trilayer construct, creating spatial control of the hinge within a single plane *i.e.* xy plane. By stacking multiple bilayer/trilayer constructs it is possible to also control the hinge location through the thickness of the construct *i.e.* in the z-direction. This approach is demonstrated through the printing of a triple bilayer/trilayer construct of a multi-layered flower (Fig. 8) where each petal can be actuated to a different extent (folding to a different actuation angle, inner petals 90°, middle petals 60° and outer petals 30°). Each bilayer/trilayer construct acts individually, enabling the hinge to be located across the individual constructs as in the designs demonstrated previously. Individual constructs are physically joined during the printing process (see ESI, Fig. S10) via an additional elastomer layer, *i.e.* at the centre, at the fourth and eighth layer of the flower. Areas between individual constructs which need to remain separate, *i.e.* the petals of the flower, are achieved through use of a buffer layer (polylactic acid, PLA), which also acts as a support layer for subsequent layers. These buffer layers were also located at the fourth and eighth layers of the flower (Fig. 8a) [56]. Once the completed part is removed from the build platform the PLA layers can be manually removed due to poor bonding with the polyurethane elastomer, caused by large differences in the print temperature of each material (PLA is printed at 190°C, polyurethane elastomer at 240°C). This interlayer fusion is caused by only partial melting of the elastomer layer below while printing the PLA layers.

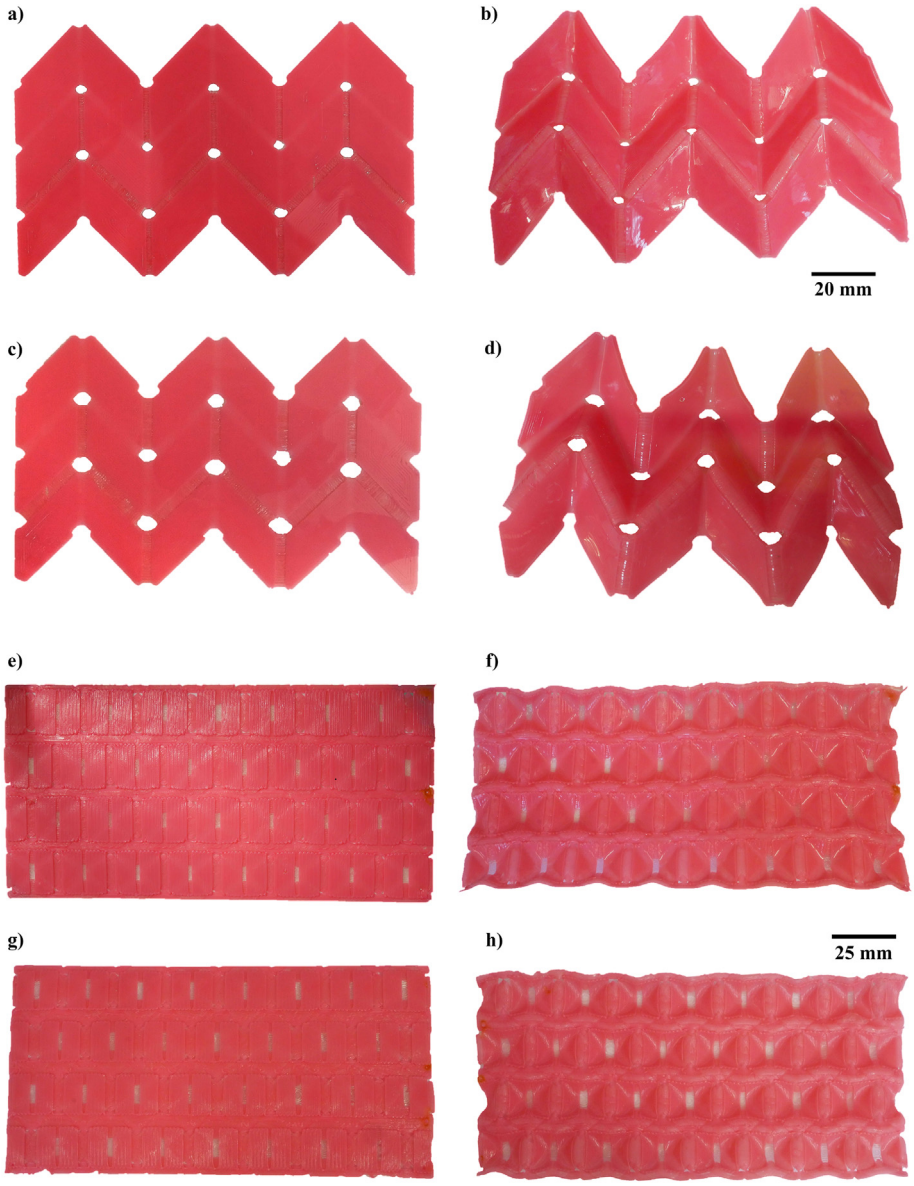

Fig. 7. Actuation of Miura-ori origami fold pattern, containing 10 vertices, from dehydrated (left) to hydrated (right); small actuation angles a) & b) and large actuation angles c) & d). Scale 1:0.59. Actuation of waterbomb origami fold pattern, containing 75 vertices, from dehydrated (left) to hydrated (right); small actuation angles e) & f) and large actuation angles g) & h). Scale 1:0.47.

The substantial difference in material stiffness aids in the separation process (Fig. 8a to b).

The demonstration of this technique beyond flat single bilayer/trilayer constructs extends the capability of this 4D printing technique to a wider range of potential designs, with the flower shown here as a simple example of how this multiple trilayer/bilayer construction approach could be used.

4. Conclusions

In this study, we have been able to demonstrate the power of this new 4D printing technique to create a range of predictable shape-changes, including designs with simple geometries, origami inspired actuation and stacked assembly. However, this hybrid 4D printing technique has the potential to be extended to create an even more diverse range of shape-changes. These could involve incorporation of techniques already demonstrated with FFF printing, including the application of a curved-layer toolpath (i.e. individual layers with variable z) to enable buckling domes [56,57]; printing on a cylindrical or inflatable print bed to create a tubular bilayer/trilayer [58], thereby enabling tubular origami designs to be created [47,59]; both enabling 3D to 3D shape-change or adding a porogen (dissolvable particles used to create a porous structure) to the hydrogel material to control the rate of actuation of the hinges and through the combination of non-porous and porous hydrogels enable sequential actuation [18,60].

In conclusion, through the use of an inexpensive commercial desktop 3D printer, readily available materials and simple bilayer/trilayer design an innovative 4D printing technique has been devised, capable of creating robust and complex origami designs, and a range of novel constructs through the use of a cheap and accessible additive manufacturing technology.

Conflicts of interest

There are no conflicts to declare.

Data availability statement

The raw/processed data required to reproduce these findings cannot be shared at this time due to technical or time limitations.

CRediT authorship contribution statement

Anna B. Baker: Conceptualization, Investigation, Methodology, Validation, Writing - original draft. **Simon R.G. Bates:** Investigation, Methodology, Writing - original draft, Writing - review & editing. **Thomas M. Llewellyn-Jones:** Software, Writing - original draft, Writing - review & editing. **Laurie P.B. Valori:** Investigation, Methodology. **Michael P.M. Dicker:** Visualization, Writing - original draft, Writing - review & editing. **Richard S. Trask:** Funding acquisition, Supervision, Writing - review & editing.

Acknowledgements

This work was supported by the Engineering and Physical Sciences Research Council (ESPRC) through the ACCIS Doctoral Training Centre grant (grant number EP/G036772/1) and the EPSRC Engineering Fellowship for Growth (grant number EP/M002489/1). MPMD is supported by the Leverhulme Trust Early Career Fellowship (grant number ECF-2017-032). The authors would like to acknowledge the kind donation of hydrogel (Tecophilic™ TPU) material from Velox GmbH and Lubrizol LifeSciences.

Appendix A. Supplementary data

Supplementary data to this article can be found online at https://doi.org/10.1016/j.matdes.2018.107544.

References

[1] S. Tibbits, 4D printing: multi-material shape change, Archit. Des. 84 (1) (2014) 116–121.
[2] S.E. Bakarich, R. Gorkin, M.I.H. Panhuis, G.M. Spinks, 4D printing with mechanically robust, thermally actuating hydrogels, Macromol. Rapid Commun. 36 (12) (Jun 2015) 1211–1217.
[3] Q. Ge, A.H. Sakhaei, H. Lee, C.K. Dunn, N.X. Fang, M.L. Dunn, Multimaterial 4D printing with tailorable shape memory polymers, Sci. Rep. 6 (1) (Nov. 2016) 31110.
[4] Y. Mao, K. Yu, M.S. Isakov, J. Wu, M.L. Dunn, H.J. Qi, Sequential self-folding structures by 3D printed digital shape memory polymers, Sci. Rep. 5 (Jan. 2015) 13616.
[5] T. van Manen, S. Janbaz, A.A. Zadpoor, Programming 2D/3D shape-shifting with hobbyist 3D printers, Mater. Horiz. 4 (6) (2017) 1064–1069.
[6] G. Villar, A.D. Graham, H. Bayley, A tissue-like printed material, Science 340 (6128) (2013) 48–52.
[7] Q. Ge, C.K. Dunn, H.J. Qi, M.L. Dunn, Active origami by 4D printing, Smart Mater. Struct. 23 (9) (Sep. 2014) 094007.
[8] M. López-Valdeolivas, D. Liu, D.J. Broer, C. Sánchez-Somolinos, 4D Printed Actuators with Soft-Robotic Functions, Macromol. Rapid Commun. 39 (5) (2018) 3–9.
[9] A. Sydney Gladman, E.A. Matsumoto, R.G. Nuzzo, L. Mahadevan, J.A. Lewis, Biomimetic 4D printing, Nat. Mater. 15 (4) (Jan. 2016) 413–418.
[10] L. Huang, R. Jiang, J. Wu, J. Song, H. Bai, B. Li, Q. Zhao, T. Xie, Ultrafast digital printing toward 4D shape changing materials, Adv. Mater. 29 (7) (Feb. 2017) 1605390.
[11] S. Naficy, R. Gately, R. Gorkin, H. Xin, G.M. Spinks, 4D printing of reversible shape morphing hydrogel structures, Macromol. Mater. Eng. 302 (1) (Jan. 2017) 1600212.
[12] F. Momeni, X. Liu, J. Ni, et al. A review of 4D printing, Mater. Des. 122 (2017) 42–79.
[13] C.K. Chua, K.F. Leong, C.S. Lim, Rapid Prototyping: Principles and Applications, 3rd ed., World Scientific Publishing Co., Inc., River Edge, NJ, USA, 2010.
[14] S.R. Bates, I.R. Farrow, R.S. Trask, 3D printed polyurethane honeycombs for repeated tailored energy absorption, Mater. Des. 112 (Dec. 2016) 172–183.
[15] H.K. Yap, H.Y. Ng, C.-H. Yeow, High-force soft printable pneumatics for soft robotic applications, Soft Rob. 3 (3) (Sep. 2016) 144–158.
[16] S. Bijadi, E. de Bruijn, E.Y. Tempelman, J. Oberdorf, Application of multi-material 3D printing for improved functionality and modularity of open source low-cost prosthetics: a case study, 2017 Design of Medical Devices Conference, ASME. Apr. 2017, pp. V001T10A003.
[17] S.R. Bates, I.R. Farrow, R.S. Trask, 3D printed elastic honeycombs with graded density for tailorable energy absorption, Active and Passive Smart Structures and Integrated Systems 2016, vol. 9799, International Society for Optics and Photonics. 2016, pp. 979907.
[18] M.P. Dicker, A.B. Baker, R.J. Iredale, S. Naficy, I.P. Bond, C.F. Faul, J.M. Rossiter, G.M. Spinks, P.M. Weaver, Light-triggered soft artificial muscles: molecular-level amplification of actuation control signals, Sci. Rep. 7 (1) (2017) 9197.
[19] H. Jia, Z. Huang, Z. Fei, P.J. Dyson, Z. Zheng, X. Wang, Bilayered polyurethane/dipole-dipole and H-bonding interaction reinforced hydrogels as thermo-responsive soft manipulators, J. Mater. Chem. B 5 (41) (2017) 8193–8199.
[20] Y. Li, H. Chen, D. Liu, W. Wang, Y. Liu, S. Zhou, pH-responsive shape memory poly (ethylene glycol)-poly (ε-caprolactone)-based polyurethane/cellulose nanocrystals nanocomposite, ACS Appl. Mater. Interfaces 7 (23) (2015) 12988–12999.
[21] E. Ho, Y. Chen, Y. Traore, A. Li, K. Fowke, Development of polyether urethane intravaginal rings for the sustained delivery of hydroxychloroquine, Drug Des. Devel. Ther. (Oct. 2014) 1801.
[22] A. Melaiye, Z. Sun, K. Hindi, A. Milsted, D. Ely, D.H. Reneker, C.A. Tessier, W.J. Youngs, Silver(I)–imidazole cyclophane gem -diol complexes encapsulated by electrospun tecophilic nanofibers: formation of nanosilver particles and antimicrobial activity, J. Am. Chem. Soc. 127 (7) (Feb. 2005) 2285–2291.
[23] E. Vatankhah, M.P. Prabhakaran, D. Semnani, S. Razavi, M. Morshed, S. Ramakrishna, Electrospun tecophilic/gelatin nanofibers with potential for small diameter blood vessel tissue engineering, Biopolymers 101 (12) (Dec. 2014) 1165–1180.
[24] A. Le Duigou, M. Castro, R. Bevan, N. Martin, 3D printing of wood fibre biocomposites: from mechanical to actuation functionality, Mater. Des. 96 (2016) 106–114.
[25] D. Han, Z. Lu, S.A. Chester, H. Lee, Micro 3D printing of a temperature-responsive hydrogel using projection micro-stereolithography, Sci. Rep. 8 (1) (2018) 1963.
[26] Z. Hu, X. Zhang, Y. Li, Synthesis and application of modulated polymer gels, Science (New York, N.Y.) 269 (5223) (Jul. 1995) 525–527.
[27] S. Zakharchenko, N. Puretskiy, G. Stoychev, M. Stamm, L. Ionov, Temperature controlled encapsulation and release using partially biodegradable thermo–magneto-sensitive self-rolling tubes, Soft Matter 6 (12) (2010) 2633.
[28] G. Stoychev, N. Puretskiy, L. Ionov, Self-folding all-polymer thermoresponsive microcapsules, Soft Matter 7 (7) (2011) 3277.
[29] K.-U. Jeong, J.-H. Jang, D.-Y. Kim, C. Nah, J.H. Lee, M.-H. Lee, H.-J. Sun, C.-L. Wang, S.Z.D. Cheng, E.L. Thomas, Three-dimensional actuators transformed from the programmed two-dimensional structures via bending, twisting and folding mechanisms, J. Mater. Chem. 21 (19) (2011) 6824.
[30] T.S. Shim, S.H. Kim, C.J. Heo, H.C. Jeon, S.M. Yang, Controlled origami folding of hydrogel bilayers with sustained reversibility for robust microcarriers, Angew. Chem. Int. Ed. 51 (6) (2012) 1420–1423.
[31] G. Stoychev, S. Turcaud, J.W.C. Dunlop, L. Ionov, Hierarchical multi-step folding of polymer bilayers, Adv. Funct. Mater. 23 (18) (May 2013) 2295–2300.
[32] S. Timoshenko, Analysis of bi-metal thermostats, J. Opt. Soc. Am. 11 (3) (Sep. 1925) 233–255.
[33] D. Morales, I. Podolsky, R.W. Mailen, T. Shay, M.D. Dickey, O.D. Velev, Ionoprinted multi-responsive hydrogel actuators, Micromachines 7 (6) (2016) 98.
[34] J.-W. Su, X. Tao, H. Deng, C. Zhang, S. Jiang, Y. Lin, J. Lin, 4D printing of a self--morphing polymer driven by a swellable guest medium, Soft Matter 14 (5) (2018) 765–772.
[35] E. Palleau, D. Morales, M.D. Dickey, O.D. Velev, Reversible patterning and actuation of hydrogels by electrically assisted ionoprinting, Nat. Commun. 4 (2013) 2257.
[36] L. Ionov, Bioinspired microorigami by self-folding polymer films, Macromol. Chem. Phys. 214 (11) (2013) 1178–1183.
[37] J. Na, A.A. Evans, J. Bae, M.C. Chiappelli, C.D. Santangelo, R.J. Lang, T.C. Hull, R.C. Hayward, Programming reversibly self-folding origami with micropatterned photo-crosslinkable polymer trilayers, Adv. Mater. 27 (1) (2015) 79–85.
[38] S.-J. Jeon, R.C. Hayward, Reconfigurable microscale frameworks from concatenated helices with controlled chirality, Adv. Mater. 29 (17) (2017) 1606111.
[39] G. Stoychev, S. Zakharchenko, S. Turcaud, J.W. Dunlop, L. Ionov, Shape-programmed folding of stimuli-responsive polymer bilayers, ACS nano 6 (5) (2012) 3925–3934.
[40] D. Dureisseix, An overview of mechanisms and patterns with origami, Int. J. Space Struct. 27 (1) (2012) 1–14.
[41] J.L. Silverberg, A.A. Evans, L. McLeod, R.C. Hayward, T. Hull, C.D. Santangelo, I. Cohen, Using origami design principles to fold reprogrammable mechanical metamaterials, Science 345 (6197) (2014) 647–650.
[42] J.L. Silverberg, J.-H. Na, A.A. Evans, B. Liu, T.C. Hull, C.D. Santangelo, R.J. Lang, R.C. Hayward, I. Cohen, Origami structures with a critical transition to bistability arising from hidden degrees of freedom, Nat. Mater. 14 (4) (2015) 389.
[43] M. Schenk, S.D. Guest, Origami folding: a structural engineering approach, Origami 5: Fifth International Meeting of Origami Science, Mathematics, and Education, CRC Press, Boca Raton, FL. 2011, pp. 291–304.
[44] B.H. Hanna, J.M. Lund, R.J. Lang, S.P. Magleby, L.L. Howell, Waterbomb base: a symmetric single-vertex bistable origami mechanism, Smart Mater. Struct. 23 (9) (2014) 094009.
[45] E.A. Peraza-Hernandez, D.J. Hartl, R.J. Malak, Jr, D.C. Lagoudas, Origami-inspired active structures: a synthesis and review, Smart Mater. Struct. 23 (9) (2014) 094001.

[46] K. Kuribayashi, K. Tsuchiya, Z. You, D. Tomus, M. Umemoto, T. Ito, M. Sasaki, Self-deployable origami stent grafts as a biomedical application of Ni-rich TiNi shape memory alloy foil, Mater. Sci. Eng. A 419 (1-2) (2006) 131–137.
[47] C. Jianguo, D. Xiaowei, Z. Ya, F. Jian, T. Yongming, Bistable behavior of the cylindrical origami structure with Kresling pattern, J. Mech. Des. 137 (6) (2015) 061406.
[48] A.B. Baker, D.F. Wass, R.S. Trask, Thermally induced reversible and reprogrammable actuation of tough hydrogels utilising ionoprinting and iron coordination chemistry, Sensors Actuators B Chem. 254 (2018) 519–525.
[49] M.T. Tolley, S.M. Felton, S. Miyashita, D. Aukes, D. Rus, R.J. Wood, Self-folding origami: shape memory composites activated by uniform heating, Smart Mater. Struct. 23 (9) (2014) 094006.
[50] T.H. Ware, M.E. McConney, J.J. Wie, V.P. Tondiglia, T.J. White, Voxelated liquid crystal elastomers, Science 347 (6225) (2015) 982–984.
[51] Z. Zhao, J. Wu, X. Mu, H. Chen, H.J. Qi, D. Fang, Origami by frontal photopolymerization, Sci. Adv. 3 (4) (Apr. 2017) e1602326.
[52] Y. Chen, R. Peng, Z. You, Origami of thick panels, Science 349 (6246) (2015) 396–400.
[53] C.D. Onal, R.J. Wood, D. Rus, An origami-inspired approach to worm robots, IEEE/ASME Trans. Mechatron. 18 (2) (2013) 430–438.
[54] D.-Y. Lee, J.-S. Kim, S.-R. Kim, J.-S. Koh, K.-J. Cho, The deformable wheel robot using magic-ball origami structure, ASME 2013 International Design Engineering Technical Conferences and Computers and Information in Engineering Conference, American Society of Mechanical Engineers. 2013, pp. V06BT07A040–V06BT07A040.
[55] Y. Chen, H. Feng, J. Ma, R. Peng, Z. You, Symmetric waterbomb origami, Proc. R. Soc. A 472 (2190) (2016) 20150846.
[56] R.J.A. Allen, R.S. Trask, An experimental demonstration of effective curved layer fused filament fabrication utilising a parallel deposition robot, Addit. Manuf. 8 (2015) 78–87.
[57] A.M. Abdullah, P.V. Braun, K.J. Hsia, Programmable shape transformation of elastic spherical domes, Soft Matter 12 (29) (2016) 6184–6195.
[58] M. Schaffner, P.A. Rühs, F. Coulter, S. Kilcher, A.R. Studart, 3D printing of bacteria into functional complex materials, Sci. Adv. 3 (12) (2017) eaao6804.
[59] J. Ma, Z. You, Modelling of the waterbomb origami pattern and its applications, ASME 2014 International Design Engineering Technical Conferences and Computers and Information in Engineering Conference, American Society of Mechanical Engineers. 2014, pp. V05BT08A047–V05BT08A047.
[60] G. Gerlach, K.-F. Arndt, Hydrogel Sensors and Actuators: Engineering and Technology, vol. 6. Springer Science & Business Media. 2009.